Lattice strain and band overlap of the thermoelectric composite $Mg_2Si_{1-x}Sn_x$

Wenliang Yao[1], Shunbo Hu[1,2*], Fanhao Jia[1,2], Jeffrey R. Reimers[1,3], Yin Wang[1,2], David J. Singh[4], and Wei Ren[1,2*]

[1] *Physics Department, International Center for Quantum and Molecular Structures, Materials Genome Institute, Shanghai University, Shanghai 200444, China*

[2] *Zhejiang Laboratory, Hangzhou 311100, China*

[3] *University of Technology Sydney, School of Mathematical and Physical Sciences, Ultimo, New South Wales 2007, Australia*

[4]*Department of Physics and Astronomy, University of Missouri, Columbia MO 65211, USA*

* *E-mail: renwei@shu.edu.cn*

shunbohu@shu.edu.cn

ABSTRACT

$Mg_2Si_{1-x}Sn_x$ solid solutions show enhanced thermoelectric performance when the Sn mole fraction x is approximately x = 0.7. This has been discussed in terms of complexity of the electronic structure arising from crossover of two bottom conduction bands, but direct detailed understanding of the origins and precise nature of this band convergence is limited. Here, we report first-principles calculations of the band edge changes analysed by band unfolding and crystal orbital Hamilton population techniques. We find that strain is particularly important at this crossing. Mg_2Si and Mg_2Sn show opposite trends in the conduction band edge shifts leading to a band crossover at $x \sim 0.625$. However, there are also important effects due to disorder. Transport calculations show that enhancement of the figure of merit ZT value owes to the combined effects of lattice strain, band edge overlap, composition change and disorder.

I. INTRODUCTION

Thermoelectric materials are of importance for future energy technologies, for example conversion of converting waste heat into electricity [1]. This requires high performance thermoelectric materials. Performance in this context is measured by a dimensionless figure of merit $ZT = S^2\sigma T/\kappa$. Here T is the temperature, S is the Seebeck coefficient, σ is the electrical conductivity, and κ is the thermal conductivity. ZT limits the energy conversion efficiency [2], such that in the limit when ZT approaches infinity the conversion efficiency of a properly designed device approaches Carnot efficiency. Optimizing to obtain high ZT is complicated by the fact that the transport parameters entering this expression are usually counter-correlated, so that for example, combinations of high electrical conductivity and high Seebeck coefficient are unusual [2,3]. Similarly, high electrical conductivity and very low thermal conductivity is a combination that is difficult to achieve. However, various concepts for resolving these contradictions and materials embodying them have been developed, including for example the "phonon-glass electron crystal" (PGEC) materials [4] and materials where complex band structures of various types overcome the limitations imposed by the counter-correlation of σ and S [5,6].

$Mg_2Si_xSn_{1-x}$ materials are of particular interest for energy technology because of their combination of high ZT, high terrestrial elemental abundant, low cost, and non-

toxic nature of its constituents. Mg_2Si and Mg_2Sn are indirect band gap semiconductors with similar band edge dispersions. $Mg_2Si_{1-x}Sn_x$ shows high *ZT* values from 0.6 to 1.3 in a mid-temperature range of 400-900 K, when appropriately doped, e.g. with Sb, to optimum carrier concentrations. This is understood as arising from a combination of alloy-disorder induced reduction in thermal conductivity and a complex band structure arising from convergence of the conduction band edges [6-10]. In this way, reasonable thermal conductivity, combined with high Seebeck coefficient and high electrical conductivity, can be simultaneously obtained [11-19]. Zaitsev *et al.* first pointed out the crossover of two conduction band edges in Mg_2Si and Mg_2Sn, which have relatively heavy or light effective masses, respectively [20]. Then, this idea was extended to their solid solutions of Mg_2Ge or Mg_2Sn with Mg_2Si as well, although better thermoelectric system was still n-type doped $Mg_2Si_{1-x}Sn_x$ [21] with a *ZT* of 1.1 at ~800 K. After that, an optimized *ZT* of 1.3 for $x \approx 0.7$ at 700 K was obtained in experiments [22]. This is a very desirable range for waste heat recovery, as it is in the range for high grade waste heat sources such as exhaust gas from internal combustion engines. In addition, a similar *ZT* of 1.3 was also reported in $Mg_{2.16}(Si_{0.4}Sn_{0.6})$ with doping by 1.5% Sb [23].

Theoretical work supports the high performance of this system [17,22], with a key reason being band overlap or degeneracy [24] at the conduction band edges in a range of x = 0.6-0.7. The dominant reason for this was ascribed to effective lattice strain in the alloy [25]. The Mg_2Si and Mg_2Sn materials may be regarded as experiencing tensile strain and compressive strain, respectively, in their solid solutions. Boltzmann transport theory calculations have been applied to show that both the Seebeck coefficient and electrical conductivity can be effectively enhanced by strain [19]. However, chemical effects other than strain and disorder could also be important. This motivates more detailed studies of the lattice strain effect on thermoelectric parameters of Mg_2Si and Mg_2Sn, in particular to understand the specific synergetic contributions of lattice strain, band overlap and composition to the enhancement of *ZT*.

With this aim, we calculate the effective band structures of $Mg_2Si_{1-x}Sn_x$ ($0 \leq x \leq 1$) solid solutions to confirm the crossover of conduction band edges accounting for the different chemical species (Si and Sn). We apply a band unfolding technique to extract the band information from a reduced Brillouin zone of the 2×2×2 supercell and project them into the first Brillouin zone of the primitive cell. This allows separation of the different contributions. After the analysis, we find that the overlap of band edges indeed happens when $x \sim 0.625$. The lattice strains corresponding to this composition ratio of 0.625 are 4.3 % for Mg_2Si and -2.6 % for Mg_2Sn, respectively.

Then, we separately investigate the tensile or compressive lattice strain effects of the Mg_2Si and Mg_2Sn. We apply a *k*-dependent crystal orbital Hamilton population (COHP) analysis [26-32] of the band structures, by which we straightforwardly follow the evolution process of the overlap of the first and second conduction bands [6]. We confirm that they both show the crossover of conduction band edges under a tensile strain of 2.1 % for Mg_2Si or a compressive strain of -4.0 % for Mg_2Sn. The changes of Seebeck coefficients, electrical conductivities, and *ZT* values caused by the lattice strain are then evaluated by performing additional Boltzmann transport theory calculations. Finally, combining the results for the two end-point compounds and their solid solutions,

we clarify the contributions of the lattice strain, band overlap, composition change and disorder to the enhanced thermoelectric performance.

II. METHODS

Our present calculations were performed within the framework of density functional theory using the projector-augmented wave (PAW) method [33] implemented in the Vienna ab initio simulation package (VASP) [34-36]. We used the Perdew-Burke-Ernzerhof (PBE) exchange correlation functional [37] with a plane wave cutoff of 520 eV. The relaxations of the supercells were done until the total energy converged within 10^{-6} eV and the force on each atom was less than 0.001 eV/Å. For most semiconductors standard semi-local density functionals, including PBE, are known to underestimate band gaps. We calculated the electronic structures using the modified Becke-Johnson (mBJ) meta-GGA potential [38,39]. This approach generally gives greatly improved band gaps, comparable to hybrid functional or GW methods but is computationally much less expensive [39-41]. This is important for transport calculations, which require electronic structures on very fine meshes within the Brillouin zone.

A series of $Mg_2Si_{1-x}Sn_x$ solid solution structures were constructed based on a 2×2×2 supercell. The Sn concentration ratio x thereby could be 0, 0.250, 0.375, 0.500, 0.625, 0.750, 0.875, and 1, covering the range of experimental measurements. The supercell band structure was unfolded to the first Brillouin zone of the pure compound using VASPKIT [42]. The band-resolved projected crystal orbital Hamilton populations (pCOHP) [29-31,43] were used to track the band crossover. The electrical transport property was calculated using Boltzmann transport theory as implemented in *Transopt* [44,45]. The Brillouin zone sampling was done using uniform k point meshes with spacings smaller than $2\pi\times0.03$Å^{-1} in order to converge the transport results.

In the calculation, the Seebeck coefficient S can be obtained from the Boltzmann transport theory as implemented in the *Transopt* code, by using the constant relaxation time approximation (CRTA) [44,45] to treat τ as a constant. Therefore, the electrical conductivity (σ) is expressed in the form of the ratio σ/τ. However, if one wants to predict a thermoelectric property like ZT, knowing τ is a must. Also, to our knowledge, there are no published or accurate data on this property for Mg_2Si and Mg_2Sn. Then, a standard electron-phonon dependence of relaxation time τ on T and n was used, namely $\tau = CT^{-1}n^{-1/3}$. Here, C is a constant determined form experimental data [46-48], to be 5×10^{-6} s·K·cm and 4.45×10^{-5} s·K·cm for n-type Mg_2Si and Mg_2Sn, respectively.

TABLE I. Calculated and experimental lattice constants a (Å) of Mg_2X (X=Si, Sn).

	Mg_2Si		Mg_2Sn		$Mg_2Si_{0.375}Sn_{0.625}$	
	This work	Other calc.	This work	Other calc.	This work	Other calc.
a	6.360	6.364[a] 6.395[b]	6.810	6.805[a] 6.856[b]	6.633	6.640[c]
Expt.	6.338-6.391[b]		6.760-6.836[b]			

[a]Ref. [16], [b]Ref. [46], [c]Ref. [47].

TABLE II. Calculated and experimental band gaps (eV) of Mg_2X (X=Si, Sn).

	Mg_2Si		Mg_2Sn	
Functional	This work	Other calc.	This work	Other calc.
mBJ	0.62	0.58-0.60[cd]	0.26	0.30[d]
PBE	0.21	0.22[f]	-0.20	-0.19[f]
HSE06	0.59	0.49[g]	0.14	0.13[g]
SCAN	0.47		0.01	
PBEsol	0.13		-0.18	
Expt.	0.69-0.78[e]		0.23-0.33[e]	

[c]Ref. [16], [d]Ref. [48], [e]Ref. [14], [f]Ref. [49], [g]Ref. [11].

III. RESULTS AND DISCUSSION

Mg_2X (X=Si, Sn) occurs in a face centered cubic structure, space group Fm-3m. Figure 1a presents the structures of Mg_2X (X=Si, Sn) in their primitive cell, translationally equivalent unit cell and in a 2×2×2 supercell. The equilibrium lattice constants of Mg_2Si and Mg_2Sn calculated by the PBE functional are 6.360 Å and 6.810 Å, respectively, which are in excellent agreement with the experiments and previous calculations (see TABLE I) [49]. Their fundamental electronic band gaps (listed in TABLE II) and band structures (shown in Figure S1) have been calculated with various functionals. The modified Becke Johnson (mBJ) potential [38,39] has been shown to give band gaps in good accord with experiment for a wide range of semiconducting materials. Importantly, we find mBJ band gaps of Mg_2Si and Mg_2Sn of 0.623 eV and 0.261 eV, respectively. These are very close to the values from experiments or GW and HSE06 calculations [49]. We present mBJ electronic structures and base our transport calculations on them.

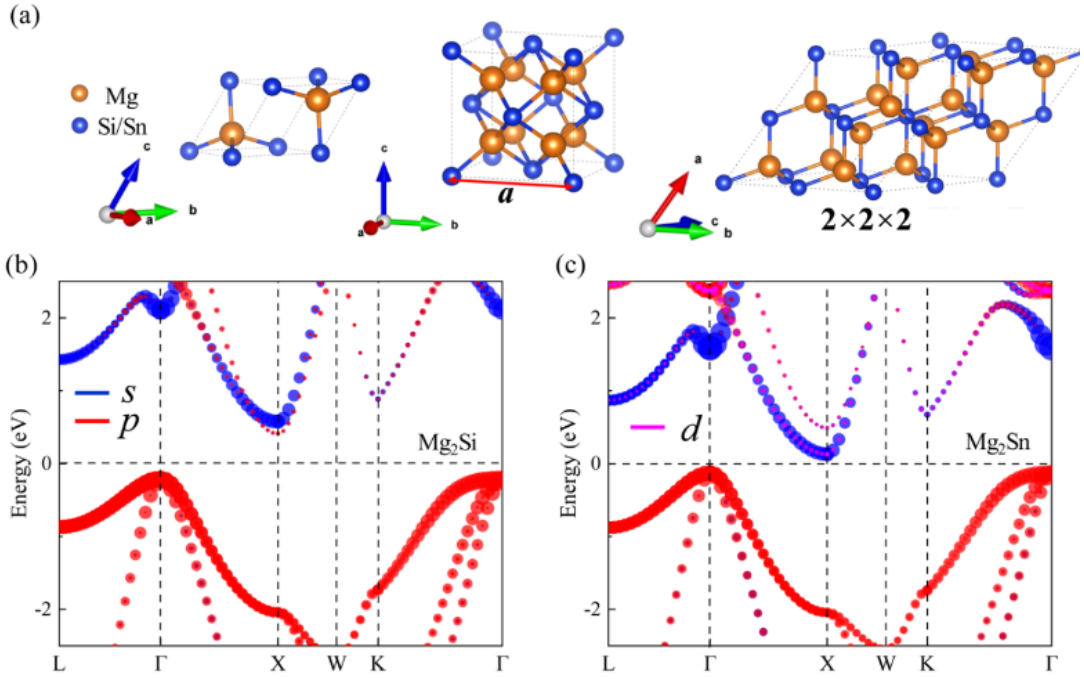

FIG. 1. (a) The schematic diagrams of crystal structures: primitive cell, unit cell and supercell of Mg_2X (X=Si, Sn). The projected (mBJ) band structures of (b) Mg_2Si and (c) Mg_2Sn from primitive cell calculations. The size of the colored dots indicates the

weights of different orbitals. The font size of the writing should be larger than 7.5 pt at the size that the journal will use … 8 or 9 is good.

The mBJ band structures of Mg_2Si and Mg_2Sn are displayed in Figure 1b and 1c, with the atomic orbital projections. Both compounds show similar band dispersions, consistent with previous reports [16]. Their indirect band gaps are defined by the energy difference between the valence band maximum (VBM) at the Γ point and conduction band minimum (CBM) at the X point. The valence bands near the band edge are from Si or Sn *p* orbitals, while the conduction bands show much stronger orbital hybridization. There are two conduction bands near the minimum of conduction band. One is dominated mostly by the *p* or *d* orbital components with lighter effective mass (0.5 m_0 for Mg_2Si and 0.58 m_0 for Mg_2Sn), while the other mostly comes from *s* orbital components with a heavier effective mass (0.69 m_0 for Mg_2Si and 1.0 m_0 for Mg_2Sn). Interestingly, these two conduction bands with different characteristics, have opposite orders in Mg_2Si and Mg_2Sn. This is the basis of the band convergence in $Mg_2Si_{1-x}Sn_x$ solid solutions.

The effective $Mg_2Si_{1-x}Sn_x$ solid solution band structures are shown in Figures 2 and S2, The Bloch states in the supercell have been unfolded into the first Brillouin zone of primitive cell. As expected, their band gaps monotonously decrease with increasing Sn content. These plots directly show the conduction band crossover at x = 0.625. This composition is very close to the range around x=0.7 where high thermoelectric performance is found. The conduction band crossover leads to a significantly natural enhanced density-of-states effective mass, which gives rise to large absolute values of the Seebeck coefficient with no adverse effect on the carrier mobility [50], moreover, $Mg_2Si_{0.375}Sn_{0.625}$ exhibits the lowest lattice thermal conductivity among all their solid solutions [17,22]. It consistent with the existing understanding that this convergence is important for the thermoelectric performance.

This raises the question of the origin of this convergence. In the following, we will clarify that this crossover is a result of the lattice strain rather just the chemical nature of the elements. This then leads to the expectation that other methods of applying strain can control the thermoelectric performance of these systems.

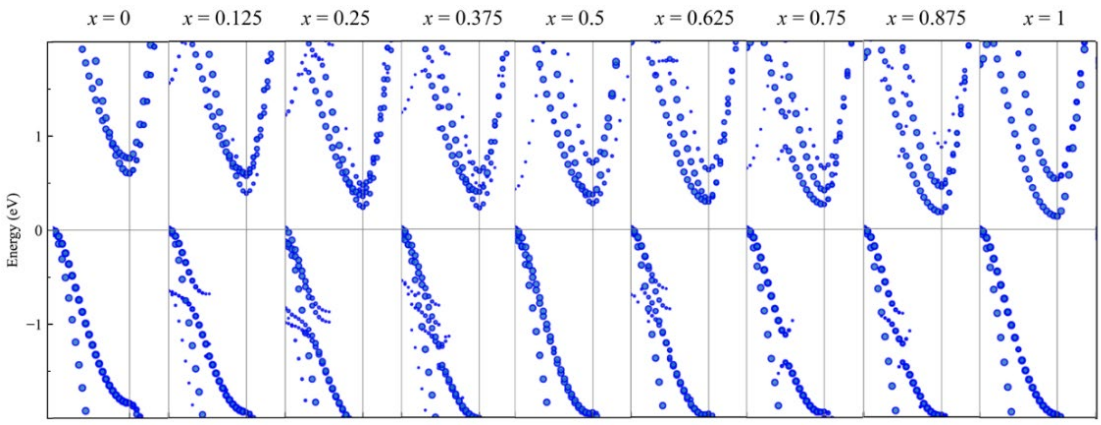

FIG. 2. The mBJ band structures of $Mg_2Si_{1-x}Sn_x$ solid solutions, which have been

unfolded into the first Brillouin zone of unit-cell along Γ-X-W. The Sn composition ratio *x* varies from 0 to 1.the writing is too small here too

TABLE III. Calculated mBJ band gaps (eV) of Mg_2X (X=Si, Sn) as function of artificial (isotropic strain) lattice constant *a* (Å). Here, I and XI represent the equilibrium lattice constants of Mg_2Si and Mg_2Sn respectively, II to X are for the extrapolated values between I and XI.

	I	II	III	IV	V	VI	VII	VIII	IX	X	XI
a (Å)	6.36	6.41	6.45	6.49	6.54	6.58	6.63	6.67	6.72	6.76	6.81
Mg_2Si	0.62	0.64	0.66	0.66	0.63	0.59	0.56	0.52	0.48	0.44	0.40
Mg_2Sn	0.38	0.41	0.44	0.46	0.46	0.42	0.39	0.36	0.32	0.29	0.26

To separate the influence of chemical identity from strain, we start with the two end-point compounds, Mg_2Si and Mg_2Sn, which have different lattice constants. Then, we constructed a series of Mg_2X (X=Si, Sn) structures with assumed lattice constants ranging from the value of 6.36 Å pertinent for Mg_2Si, to the value of 6.81 Å pertinent for Mg_2Sn, labeled in order by a set of Greek letters. The used lattice constants and the corresponding mBJ band gaps are summarized in Table III. The band gap of Mg_2Si first increases as the lattice constant is increased from 6.36 Å to 6.45 Å, and then decreases between 6.49 Å and 6.81 Å. Similar to this trend, the Mg_2Sn band gap also first increases then decreases during these ranges. This reflects the different behavior of the two bands near the conduction band minimum.

We applied a band-resolved pCOHP analysis [31,43] shown in Figure 3 to clarify the band dependence. We focus on the Mg-3*s* character, which differs between the two bands and which is important in the band formation. This unoccupied *s* orbital is very sensitive to volume. The position of the Mg 3*s* dominated band relative to the other conduction band is opposite in the two compounds, and so while both Mg_2Si and Mg_2Sn show band crossover under strain, the sign of the lattice strain to achieve this band crossover is opposite. As a result, they coincidentally have the conduction band overlaps at a similar lattice constant near 6.49 Å and 6.54 Å. Thus, strain can play an essential role in the solid solutions for the enhanced thermoelectric properties and it can be expected that other chemical and/or physical methods of applying strain can improve the thermoelectric properties of these materials.

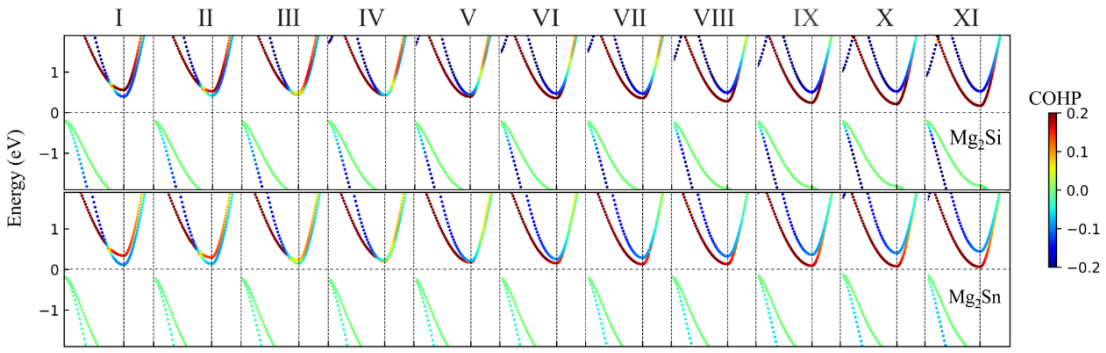

FIG. 3. The mBJ band structures along Γ-X-W of Mg_2X (X=Si, Sn) with extrapolated lattice constants listed in Table III. The COHP of Mg-3*s* is indicated by the color bar, where the blue and red mean bonding and anti-bonding state contributions, respectively. Check font sizes

Because the lattice strain can effectively change the band structure, it should have direct effects on the Seebeck coefficient S and electrical conductivity σ. The strain dependences of S and σ are displayed in Figures S3-S9. These two parameters are calculated using Boltzmann transport equations with relaxation time approximation [45]. The final thermoelectric property is determined by the optimal value of ZT that reflects the effectiveness of the material. As mentioned in the introduction, ZT is inversely proportional to the thermal conductivity κ which depends on both temperature T and carrier concentration n. It is never easy to predict κ from ab initio calculations or molecular simulations, which may even involve the effect of strain in the study. The thermal conductivities are therefore adopted to the experimental values as summarized in Table SI. A temperature of 700 K and an electron density of $n = 1.8 \times 10^{20}$ cm^{-3} are used to allow comparison with experiments. Finally, the strain dependence of thermoelectric ZT value of both Mg_2Si and Mg_2Sn is displayed in Figures 4, S10-S11. We obtain optimal ZT values of 0.13 (Mg_2Si) and 0.97 (Mg_2Sn) with lattice constants of 6.49 Å and 6.54 Å, respectively. It is clear that the lattice strain can enhance their thermoelectric performance at the same time as achieving the band crossover. The lattice strain (or band crossover) is able to enhance the ZT value of Mg_2Si form 0.13 (6.36 Å) to 0.16 (6.49 Å), with an increase about 23 %. Remarkably, the ZT value of Mg_2Sn is enhanced from 0.44 (6.81 Å) to 0.97 (6.54 Å) with a dramatic increase about 220 %. Thereby, Mg_2Sn shows both higher natural thermoelectric performance and larger turnability than the Mg_2Si from an electronic point of view.

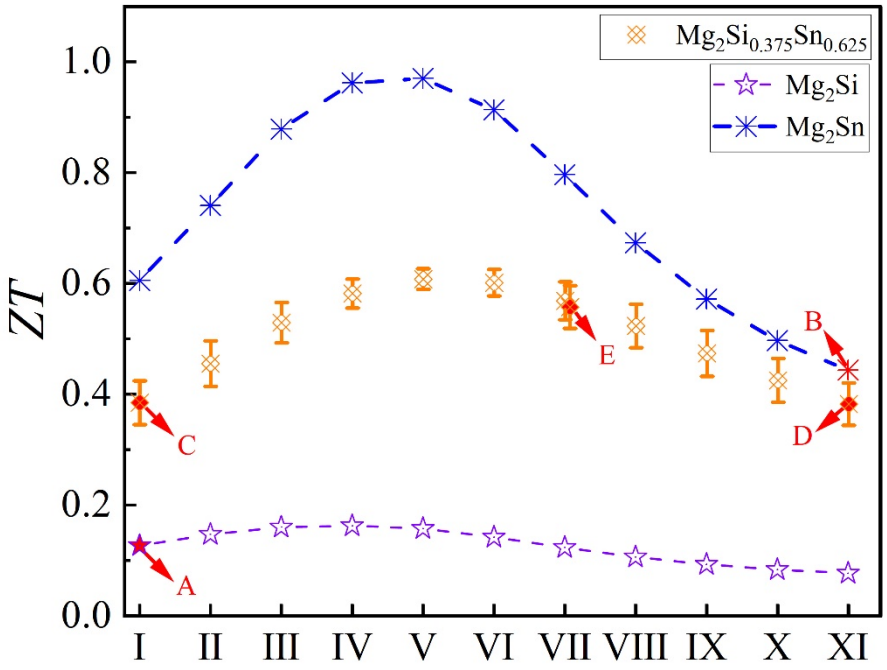

FIG. 4. Calculated *ZT* values of Mg_2Si (I) and Mg_2Sn (XI) as function of artificial lattice constant at the temperature fixed to 700 K. A, B and E indicate Mg_2Si, Mg_2Sn and $Mg_2Si_{0.375}Sn_{0.625}$ at their respective relaxed equilibrium lattice constants. C and D represent constrained "$Mg_2Si_{0.375}Sn_{0.625}$" with lattice constants fixed to that of Mg_2Si (A), and Mg_2Sn (B) respectively. The error bars are from the influence of local atomic arrangements of Si and Sn in the $Mg_2Si_{0.375}Sn_{0.625}$ supercell.

In order to separate the composition effect and the lattice strain effect, we consider in Figure 4 optimized $Mg_2Si_{0.375}Sn_{0.625}$ systems (E), as well as systems with the lattice constants constrained to the values appropriate for Mg_2Si (A) and for Mg_2Sn (B). The transport parameters at different temperatures for $Mg_2Si_{0.375}Sn_{0.625}$ disordered structures (Figure S12), taking the lattice constants into account, are shown in Figures S13-S25. For better comparison, we also use this set of lattice parameters to calculate *ZT* values for Mg_2Si and Mg_2Sn, where the relaxation time was an average value taken from Ref [17]. Is the above rewording correct? We found that the strain-free structure has a *ZT* value in the range of 0.52-0.60. The uncertainty comes from the disorder effect, i.e. there are various local atomic orderings of Si and Sn atoms in the supercell. The disorder can also play an important role in their thermoelectric performance, both from the point of view of the effect on electronic structure and presumably from alloy scattering of phonons.

To understand impacts of highly disordered structure and lattice strain for $Mg_2Si_{1-x}Sn_x$, the band structures of $Mg_2Si_{0.375}Sn_{0.625}$ under different lattice constants are shown

in Figures S26-28. When the lattice is fixed to the lattice constant of Mg_2Si, the calculated *ZT* values of the solid solutions are reduced to the range of 0.34-0.41. When the lattice is fixed to the lattice constant of Mg_2Sn, the calculated *ZT* values of the solid solutions are in the range of 0.35-0.38. By comparing relaxed Mg_2Si and constrained $Mg_2Si_{0.375}Sn_{0.625}$ under the same lattice constants of Mg_2Si in Figure 4, By comparing (Figure 4) Mg_2Si and $Mg_2Si_{0.375}Sn_{0.625}$ at the lattice structure appropriate for Mg_2Si, one finds that a composition change form x = 0 to x = 0.625 enhances the *ZT* value by about 3 fold. On the other hand, by comparing (Figure 4) Mg_2Sn and $Mg_2Si_{0.375}Sn_{0.625}$ at the lattice constants appropriate for Mg_2Sn, the composition change form x = 1 to x = 0.625 decreases the *ZT* value by about 17%. These changes are not mainly due to the conduction band overlap as this is absent in relaxed Mg_2Si, Mg_2Sn and constrained $Mg_2Si_{0.375}Sn_{0.625}$. The contribution of lattice strain can be determined by comparing relaxed and constrained $Mg_2Si_{0.375}Sn_{0.625}$. The relaxed $Mg_2Si_{0.375}Sn_{0.625}$ has overlap of the bands at the conduction band edge. Thus, based on the calculated results, both strain and band overlap are important this solid solution system.

IV. CONCLUSIONS

In this work, we have performed first principles calculations to understand the large enhancement of thermoelectric performance in $Mg_2Si_{1-x}Sn_x$ solid solutions, in particular in relation to the evolution of the band structure. Band unfolding and COHP confirm the band crossover in Mg_2Si, Mg_2Sn and their solid solutions and the origin of this. The *ZT* values were calculated using Boltzmann transport theory and are consistent with experimental reports. Compared to Mg_2Si, intrinsically Mg_2Sn has much higher natural thermoelectric performance and larger turnability. We conclude that the enhancement of *ZT* value in $Mg_2Si_{0.375}Sn_{0.625}$ is a collective result of lattice strain, band edge overlap, composition change and disorder, and not just the band convergence itself.

ACKNOWLEDGEMENTS

This work was supported by the National Natural Science Foundation of China (Grants No. 12074241, No. 11929401, No. 52130204), the Science and Technology Commission of Shanghai Municipality (Grants No. 19010500500, No. 20501130600, and No. 21JC1402600), Key Research Project of Zhejiang Lab (No. 2021PE0AC02), and High Performance Computing Center, Shanghai University.

REFERENCE

[1] Lon E. Bell, Science **321**, 1457 (2008).

[2] C. Wood, Reports on Progress in Physics **51**, 459 (1988).

[3] Boris Kozinsky and David J. Singh, Annual Review of Materials Research **51**, 565 (2021).

[4] G. S. Nolas, D. T. Morelli, and T. M. Tritt, Annual Review of Materials Science **29**, 89 (1999).

[5] Guangzong Xing, Jifeng Sun, Yuwei Li, Xiaofeng Fan, Weitao Zheng, and David J. Singh, Physical Review Materials **1**, 065405 (2017).

[6] Jiong Yang, Lili Xi, Wujie Qiu, Lihua Wu, Xun Shi, Lidong Chen, Jihui Yang, Wenqing Zhang, Ctirad Uher, and David J Singh, npjComputational Materials **2**, 15015 (2016).
[7] LiDong Zhao, ShihHan Lo, Yongsheng Zhang, Hui Sun, Gangjian Tan, Ctirad Uher, C. Wolverton, Vinayak P. Dravid, and Mercouri G. Kanatzidis, Nature **508**, 373 (2014).
[8] G. Jeffrey Snyder and Eric S. Toberer, Nature Materials **7**, 105 (2008).
[9] Yinglu Tang, Zachary M. Gibbs, Luis A. Agapito, Guodong Li, Hyun-Sik Kim, Marco Buongiorno Nardelli, Stefano Curtarolo, and G. Jeffrey Snyder, Nature Materials **14**, 1223 (2015).
[10]Y. Pei, X. Shi, A. LaLonde, H. Wang, L. Chen, and G. J. Snyder, Nature **473**, 66 (2011).
[11]Kim Chang-Eun, Soon Aloysius, and Stampfl Catherine, Physical Chemistry Chemical Physics **18**, 17 (2015).
[12]G. Busch and U. Winkler, Physica **20**, 1067 (1954).
[13]Peter M. Lee, Physical Review **135**, A1110 (1964).
[14]M. Y. Au-Yang and Marvin L. Cohen, Physical Review **178**, 1358 (1969).
[15]J. L. Corkill and M. L. Cohen, Physical Review B **48**, 17138 (1993).
[16]J. J. Pulikkotil, D. J. Singh, S. Auluck, M. Saravanan, D. K. Misra, A. Dhar, and R. C. Budhani, Physical Review B **86**, 155204 (2012).
[17]X. J. Tan, W. Liu, H. J. Liu, J. Shi, X. F. Tang, and C. Uher, Physical Review B **85**, 205212 (2012).
[18]K. Kutorasiński, J. Tobola, and S. Kaprzyk, Journal of Computational Chemistry **87**, 195205 (2013).
[19]N. Hirayama, Y. Imai, and N. Hamada, Journal of Applied Physics **127**, 205107 (2020).
[20]M. I. Fedorov V. K. Zaitsev, A. T. Burkov, E. A. Gurieva, I. S. Eremin, P. P. Konstantinov, S. V. Ordin, S. Sano, and M. V. Vedernikov, in Proceedings of the 24th International Conference on Thermoelectrics (IEEE), 151 (2002).
[21]V. K. Zaitsev, M. I. Fedorov, E. A. Gurieva, I. S. Eremin, P. P. Konstantinov, A. Yu Samunin, and M. V. Vedernikov, Physical Review B **74**, 045207 (2006).
[22]Wei Liu, Xiaojian Tan, Kang Yin, Huijun Liu, Xinfeng Tang, Jing Shi, Qingjie Zhang, and Ctirad Uher, Physical Review Letters **108**, 166601 (2012).
[23]Wei Liu, Xinfeng Tang, Han Li, Kang Yin, Jeff Sharp, Xiaoyuan Zhou, and Ctirad Uher, Journal of Materials Chemistry **22**, 13653 (2012).
[24]Yabei Wu, Weiyi Xia, Weiwei Gao, Wei Ren, and Peihong Zhang, Physical Review Applied **8**, 034007 (2017).
[25]Chang-Eun Kim, Aloysius Soon, and Catherine Stampfl, Physical Chemistry Chemical Physics **18**, 939 (2016).
[26]V. Popescu and A. Zunger, Physical Review Letters **104**, 236403 (2010).
[27]Voicu Popescu and Alex Zunger, Physical Review B **85**, 085201 (2012).
[28]W. Ku, T. Berlijn, and C. C. Lee, Physical Review Letters **104**, 216401 (2010).
[29]V. L. Deringer, AL Tchougréeff, and R. Dronskowski, The Journal of Physical Chemistry A **115**, 5461 (2011).
[30]Richard Dronskowski and Peter E. Bloch, The Journal of Physical Chemistry **97**,

8617 (1993).
[31]S. Maintz, V. L. Deringer, AL Tchougréeff, and R. Dronskowski, Journal of Computational Chemistry **34**, 2557 (2013).
[32]Xin Sun, Xin Li, Jiong Yang, Jinyang Xi, Ryky Nelson, Christina Ertural, Richard Dronskowski, Weishu Liu, Gerald J. Snyder, David J. Singh, and Wenqing Zhang, Journal of Computational Chemistry **40**, 1693 (2019).
[33]P. E. Blochl, Physical Review B **50**, 17953 (1994).
[34]G. Kresse and J. Hafner, Physical Review B **47**, 558 (1993).
[35]G. Kresse and J. Hafner, Physical Review B **49**, 14251 (1994).
[36]G. G. Kresse and J.J. Furthmüller, Physical Review B **54**, 11169 (1996).
[37]G. Kresse and D. Joubert, Physical Review B **59**, 1758 (1999).
[38]Axel D. Becke and Erin R. Johnson, The Journal of Chemical Physics **124**, 221101 (2006).
[39]F. Tran and P. Blaha, Physical Review Letters **102**, 226401 (2009).
[40]David Koller, Fabien Tran, and Peter Blaha, Physical Review B **83**, 195134 (2011).
[41]David J. Singh, Physical Review B **82**, 205102 (2010).
[42]Vei Wang, Nan Xu, Jincheng Liu, Gang Tang, and Wentong Geng, Computer Physics Communications **267**, 108033 (2021).
[43]R. Nelson, C. Ertural, J. George, V. L. Deringer, G. Hautier, and R. Dronskowski, Journal of Computational Chemistry **41**, 1931 (2020).
[44]Jiong Yang, L. Xi, W. Zhang, L. D. Chen, and Jihui Yang, Journal of Electronic Materials **38**, 1397 (2009).
[45]Xin Li, Zhou Zhang, Jinyang Xi, David J. Singh, Ye Sheng, Jiong Yang, and Wenqing Zhang, Computational Materials Science **186**, 110074 (2021).
[46]Aleksandr Chernatynskiy and Simon R. Phillpot, Physical Review B **92**, 064303 (2015).
[47]Xiaojian Tan, Yinong Yin, Haoyang Hu, Yukun Xiao, Zhe Guo, Qiang Zhang, Hongxiang Wang, Guoqiang Liu, and Jun Jiang, Annalen der Physik **532**, 1900543 (2020).
[48]P. Boulet and M. C. Record, The Journal of Chemical Physics **135**, 234702 (2011).
[49]Byungki Ryu, Sungjin Park, Eun-Ae Choi, Johannes de Boor, Pawel Ziolkowski, Jaywan Chung, and Su Dong Park, Journal of the Korean Physical Society **75**, 144 (2019).
[50]H. Tamaki, H. K. Sato, and T. Kanno, Adv Mater **28**, 10182 (2016).